Transporting the Optical Chirality through the Dynamical Barriers in Optical Microcavities

Shuai Liu, Jan Wiersig, Wenzhao Sun, Yubin Fan, Li Ge, Jinkyu Yang, Shumin Xiao,* Qinghai Song,* and Hui Cao*

In mixed phase space structures, the stable islands and chaotic sea are separated by dynamical barriers. Considering the small tunneling rate, intuitively, the properties of long-lived resonances within stable islands are supposed to be less affected by the perturbations in chaotic sea. Here, the modifications on the chaotic sea which can be transported through dynamical barriers and strongly affect long-lived resonances within stable islands are experimentally demonstrated. In waveguide-connected quadruple microdisks (WCQMs), the finite orbital angular momentum and the propagation directions of long-lived resonances within stable islands could be changed and controlled by the waveguides connecting to the chaotic sea. The numerical calculations and the corresponding 4 × 4 non-Hermitian Hamiltonian theoretical model match the experimental results well and demonstrate the essential roles of asymmetrical scattering in the chaotic sea and chaotic-to-regular tunneling. This research will be interesting for fundamental studies on quantum chaos and practical applications in optical sensing.

1. Introduction

Microdisk lasers have been widely accepted as ideal platforms for fundamental researches on quantum-classical and ray-wave correspondence.[1–3] In principle, their internal ray and wave dynamics can be drastically changed from regular states to chaos by increasing the deformation parameter.[2] Meanwhile, laser emissions from microdisks can carry internal information to far field and simplify the optical characterization.[3,4] In the past decades, many types of deformed microdisks have been proposed and experimentally fabricated to study the fundamental problems such as unidirectional laser emission,[5] dynamical tunneling,[6–14] mode coupling,[15,16] optical chirality,[17–22] and even parity-time symmetry.[23,24] Among these microdisks, slightly deformed microdisk lasers are particularly interesting owing to their mixed phase space structures. The regular states can confine light for a long time (τ) via total internal reflection and produce relatively high quality factors ($Q = \omega\tau$, ω is the resonant frequency). The trajectory of light in the chaotic sea follows the unstable manifolds and rapidly transmits out along particular directions.[25] Classically, the regular states and chaotic sea are separated by the dynamical barriers.[26] The classical trajectories or rays confine independently in regions of classical phase space and cannot penetrate the barriers. In quantum or wave systems, they are connected by dynamical tunneling.[6–14] The dynamical tunneling in optical microcavities with mixed phase space structures have been thoroughly studied by many groups. In 2010, Shinohara et al. have observed the theoretically predicted directional emissions of long-lived resonances within stable islands, which

S. Liu, W. Sun, Y. Fan, S. Xiao, Dr. Q. Song
State Key Laboratory on Tunable laser Technology, Ministry of Industry and Information Technology Key Lab of Micro-Nano Optoelectronic Information System, Shenzhen Graduate School
Harbin Institute of Technology
Shenzhen 518055, P. R. China
E-mail: shumin.xiao@hit.edu.cn; qinghai.song@hit.edu.cn

J. Wiersig
Institut für Theoretische Physik, Otto-von-Guericke-Universität
Magdeburg, Postfach 4120
D-39016, Magdeburg, Germany
E-mail: jan.wiersig@ovgu.de

The ORCID identification number(s) for the author(s) of this article can be found under https://doi.org/10.1002/lpor.201800027

DOI: 10.1002/lpor.201800027

L. Ge
Department of Engineering Science and Physics
College of Staten Island
The City University of New York, Staten Island
NY 10314, USA

L. Ge
The Graduate Center
The City University of New York
NY 10016, USA

J. Yang
Department of Optical Engineering
Kongju National University
Cheonan 330717, South Korea

S. Xiao, Dr. Q. Song
Collaborative Innovation Center of Extreme Optics
Shanxi University
Taiyuan 030006, P. R. China

H. Cao
Department of Applied Physics
Yale University
New Haven, CT 06520, USA

is one of the most decisive experimental evidences for dynamical tunneling in optical systems.[12] Subsequently, the resonance assisted tunneling and the tunneling induced highly directional laser emissions have been widely studied in many systems with mixed phase space structures.[27–29]

Till now, most of the experiments on microlasers are focusing on the regular-to-chaotic tunneling.[6–13,27–29] The reversal process, that is, the chaotic-to-regular tunneling, has been rarely studied in microdisk lasers. This is mainly due to the openness and the chaotic characteristics of the microcavities. Compared with the waves within the stable islands, the tunneled light only propagates in the chaotic sea for a very short time. Meanwhile, due to the chaotic nature, the reflected light has abundant selections in chaotic sea rather than tunneling back to stable islands. Consequently, while the rate of chaotic-to-regular tunneling is as large as its time-reversal process, the tunneled light is supposed to have a small chance to return to the stable islands and the resonant behaviors of long-lived resonances in stable islands are less affected by the changes in chaotic sea. Recently, in a deformed Reuleaux triangle cavity, Ryu et al. have considered the chirality induced by the chaotic sea.[30] However, the obtained chirality is too small and the fundamental mechanism is still not clear. In contrast to this intuitive picture, we show in the current work that the resonances in stable islands can be strongly affected by asymmetric scattering in the chaotic sea and the chaotic-to-regular tunneling.

2. Experimental Section

2.1. Numerical Simulation

In the numerical simulation, we use finite-element method (FEM, COMSOL Multiphysics 4.3a) to calculate the resonant modes with eigenfrequency study. As the in-plane dimension was much larger than the thickness of the microcavity, the microcavity was approximated as a 2D object with the effective refractive index n. Outside was air with $n = 1$ and the perfect matched layer (PML) was used to absorb the outgoing waves. The Q factor was determined as $Q = f_{real}/2f_{imag}$, where f_{real} and f_{imag} were the real and imaginary parts of the calculated eigenfrequency with $f = f_{real} + i \cdot f_{imag}$. The far field patterns (FFPs) were recorded by calculating the power flux density along the inner circle of the PML.

2.2. Sample Fabrication

The samples were fabricated with standard photoresist SU8 film doped with 0.8% Rhodamine B in weight.[31,32] After 10 min exposure in ultraviolet light, a 300 nm PMMA film was spin-coated onto the SU8 film. The cavities were patterned with electron-beam lithography and developed in MIBK for 50 s. Then a 100 nm silica film was evaporated and lifted off using PG remover, leaving a silica mask on the SU8 film. At last, the samples were obtained with inductively coupled plasma etching. More details are shown in part-I, Supporting Information.

2.3. Sample Measurement

The samples were placed on a 3D translation stage and pumped by a frequency-doubled Nd:YAG laser (532 nm, 7 ns pulse duration). During the experiment, the focused laser spot was fixed at 180 μm in diameter. The emitted laser was collected by a lens and coupled into the spectrometer (Princeton instrument). The distance between lens and sample was fixed at 100 mm, which was far enough to keep the collection efficiency not changed with slight shifts in pumping configurations. FFPs were measured using a rotation stage underneath the sample. More details and the corresponding optical setup are shown in part-II, Supporting Information.

3. Results and Discussion

3.1. Numerical Calculations

We take the quadrupole shaped microcavity as an example to illustrate this effect. **Figure 1**a depicts the schematic picture of the cavity, which is a quadrupole microcavity connected with a channeling waveguide. The cavity boundary is defined by the equation $\rho\ (\phi) = R(1 + \varepsilon \cos(2\phi))$ in polar coordinates. Here, R and ε are the size and shape deformation parameters. The channeling waveguide with width w is connected to the cavity at $\phi = 0.201\pi$. For simplicity, the deformation parameter, and the width of waveguide in this research are fixed at $\varepsilon = 0.08$ and $w = 0.2$R, respectively. The ray dynamics of quadrupole cavity have been thoroughly studied and can be conveniently visualized in 2D phase space, the so-called Poincaré surface of section (PSOS), by recoding the scaled angular momentum $\sin\chi$ and the bouncing position ϕ (see Figure 1a). As shown in Figure 1b, the phase space structure of the quadrupole cavity consists of unbroken Kolmogorov–Arnold–Moser curves close to $\sin\chi = 1$ and stable islands that are surrounded by a chaotic sea at lower $\sin\chi$. While the quasi-whispering gallery modes (WGMs) with $\sin\chi$ close to 1 are better confined than other modes in the quadrupole cavity, their Q factors are strongly degraded after the connection of channeling waveguide. Consequently, the diamond resonances confined within period-4 stable islands can be experimentally excited to investigate the tunneling between stable islands and chaotic sea.[13]

In high refractive index WCQMs, the wave phenomena of diamond modes have been well explored. After a relatively long confinement, the resonances within stable islands enter the chaotic sea via dynamical tunneling and are efficiently collected by the channeling waveguides. Interestingly, while the chaotic-to-regular tunneling has not been considered, the experimental results match the analysis and numerical calculations well. For a microcavity with lower refractive index such as $n = 1.56$ for negative photoresist SU8, the period-4 stable islands are directly cut by the critical line (see Figure 1b). Intuitively, the resonances within period-4 stable islands should be much simpler. Their decay channels and FFPs are mainly determined by the transmission within stable islands. The influences of regular-to-chaotic tunneling are supposed to be negligible, let alone the chaotic-to-regular tunneling.

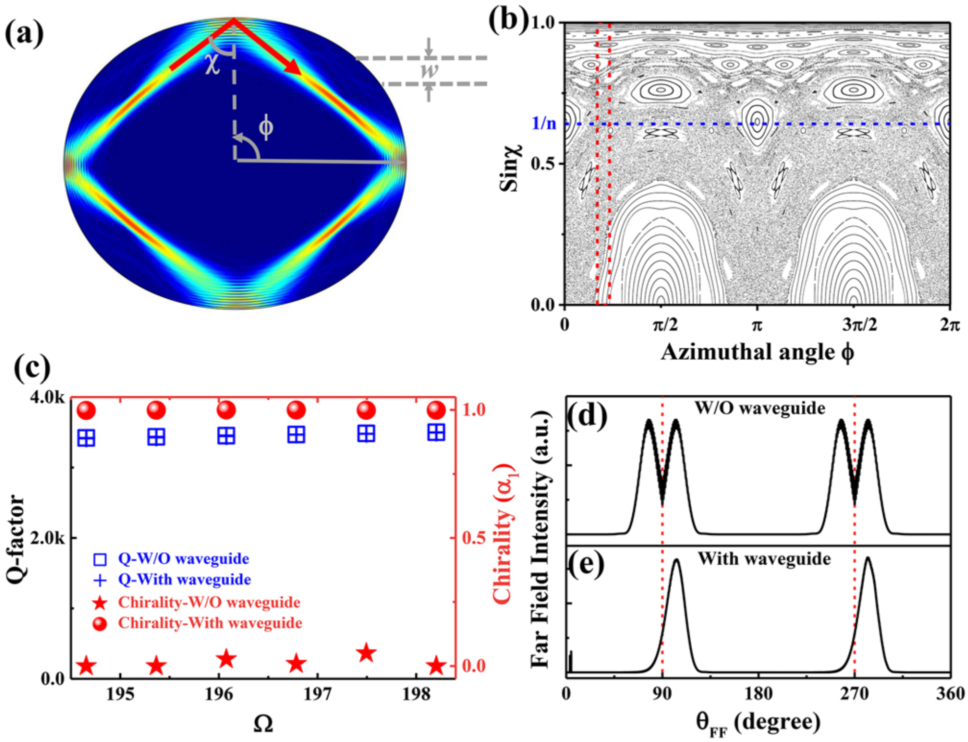

Figure 1. Numerical results for a WCQM. a) The schematic picture of the WCQM. The field pattern of a diamond mode at $\Omega = 196.07$ is overlaid. b) The PSOS of the quadrupole microcavity. The dashed red box shows the waveguide-cavity joint position in phase space. c) The numerically calculated Q and chirality as a function of Ω. Considering the experiment below, only transverse magnetic (TM, the electric field E is perpendicular to the plane) polarization is considered. d,e) The numerically calculated FFPs of the diamond in quadrupole cavity without and with channeling waveguide.

To check this intuitive picture, we have calculated the diamond modes numerically along period-4 stable islands in quadrupole microcavity with a finite element method. As shown in Figure 1c, the diamond modes in quadrupole microcavity with $n = 1.56$ have Q factors around 3400–3450. The normalized frequency is defined as $\Omega = 2\pi R/\lambda$. After the connection of channeling waveguide, the resonances are still confined along the diamond orbit (see Figure 1a) and their Q factors are only degraded by less than 1%. Such a slight degradation shows the tiny influences of conventional chaotic assisted tunneling, which is consistent with the above analysis. However, once the FFPs are taken into account, significant differences can be clearly observed. For a typical quadrupole microcavity, four directional outputs along $\theta_{FF} \approx 80°$, 100°, 260°, and 280° can be clearly seen in the FFP (see Figure 1d). Once the channeling waveguide is added, only two directional emissions beams at $\theta_{FF} \approx 100°$ and 280° have been obtained. The changes in far-field patterns are quite different from the intuitive picture. As the stable islands and chaotic sea are separated by dynamical barriers, the changes in chaotic sea thus have the possibility of being transported through the dynamical barrier and significantly affect the optical confinements within islands.

In order to explore the exact influences on diamond modes, we have projected the wave functions along the boundary of quadrupole microcavity into phase space via the Husimi functions.[33] **Figure 2**a shows the Husimi map of mode-4 in a quadrupole microcavity without channeling waveguide. We can see that both of the clockwise (CW, $\sin\chi < 0$) and counter-clockwise (CCW, $\sin\chi > 0$) components are confined along period-4 islands. Because the stable islands are directly cut by the critical line at $\phi = 0$ and π, the CCW waves refract out along $\theta_{FF} \approx 80°$ (at $\phi = 0$) and 260° (at $\phi = \pi$), whereas the CW components refract along $\theta_{FF} \approx 280°$ (at $\phi = 0$) and 100° (at $\phi = \pi$). Due to the balance between CW and CCW components, four directional outputs can be generated (see Figure 1d). Most importantly, the Husimi maps have simply demonstrated the correspondence between the FFPs and the internal field distributions. Following the correspondence, it is easy to deduce from the bidirectional emission in Figure 1e that the CW components of electromagnetic waves in quadrupole microcavity are much stronger than their CCW counterparts.

The above deduction can be verified by the Husimi map of diamond mode in a quadrupole microcavity with a channeling waveguide. As shown in Figure 2b, the period-4 stable islands can be clearly seen in the CW domain of phase space. The islands are cut by the critical line at $\phi = 0, \pi$ and bidirectional outputs are formed. The stable islands in the CCW domain of phase space, however, are more than an order of magnitude lower and thus the emissions along $\theta_{FF} \approx 80°$ and 260° disappear in the FFP. All of these results are consistent with the above analysis and demonstrate the formation of optical chirality in stable islands. Following the definition of chirality, the chirality in Husimi map can be defined as $\alpha_1 = 1 - \frac{\sum_{CCW} \text{Husimi}}{\sum_{CW} \text{Husimi}}$.[20] The chirality in Figure 2a,b are 0.009 and 0.999, respectively. Similarly, the chirality of all modes from $\Omega = 194.7$–198.2 are summarized as stars and dots in Figure 1c. The chirality (α_1) of diamond modes in

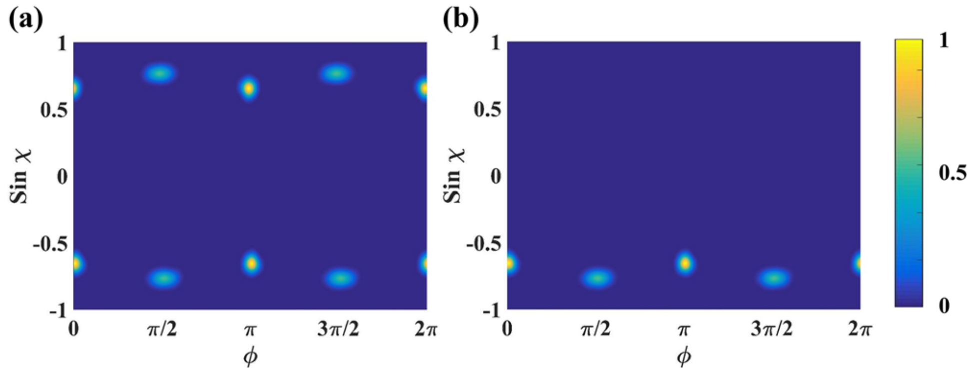

Figure 2. Husimi maps of the mode at $\Omega = 196.07$ in Figure 1c in quadrupole microdisk a) without and b) with channeling waveguide.

conventional quadrupole cavity is close to 0, consistent with the mirror-reflection symmetry of its cavity shape. The slight deviation is caused by the mesh in numerical simulation. Once the channeling waveguide is connected, their chirality is significantly increased to around 1.

3.2. Experimental Results

Based on the above numerical calculation and theoretical analysis, we have experimentally fabricated the WCQMs to check the influences of the changes in the chaotic sea on the modes in the stable islands. **Figure 3**a shows the top-view scanning electron microscope (SEM) image of a quadrupole microdisk with a connected waveguide. All of the size and deformation parameters are the same as the design in Figure 1. By placing the sample onto a rotational translation stage under a home-built optical microscope, the optical properties of the WCQMs have been recorded (see part-II, Supporting Information). When the power was low, a broad photoluminescence peak has been observed. As the pumping power was increased to 26.7 μJ, periodic narrow peaks emerged and quickly dominated the emission spectrum at higher pumping power (see Figure 3b). The dots in the inset of Figure 3b show the integrated output intensity as a function of pumping power. At the beginning, the output intensity increases slowly with the increase of pumping power. Once discrete peaks appear, a dramatic increase in the power slope is also observed, confirming the lasing actions within WCQMs well.

Following the definition of free spectral range ($\Delta\lambda = \lambda^2/n_g L$, here n_g is the group refractive index, see part-III, Supporting Information), the diamond modes along period-4 islands can be confirmed with their free spectral range of ≈2.06 nm (see part-III, Supporting Information). Then angular-resolved laser spectra have been recorded by rotating the translational stage under the microscope. Based on the mode spacing, the FFPs of diamond modes can be distinguished from the FFPs of quasi-WGMs. The experimental results are plotted in Figure 3c. Two directional laser emissions can be clearly seen along $\theta_{FF} = 94°$ and 274°. The other two directional laser beams are around ten times smaller. Based on the correspondence between the FFP and the internal mode confinement in Figure 2, we know that the diamond modes in WCQMs are dominated by the CW waves.

As a control experiment, we have fabricated a quadrupole microdisk without channeling waveguide (see Figure 3d) and studied its optical characteristics. Here, the jagged boundary is used to destroy the quasi-WGMs and excite the diamond modes experimentally. The Q factors and chirality are barely affected (see part-III, Supporting Information). Similar to the results in Figure 3b, lasing actions along the diamond orbit can be confirmed from their emission spectra and threshold behaviors in Figure 3e. By rotating the translational stage, we have also measured the angular-resolved laser spectrum and achieved the far-field patterns of diamond modes. As shown in Figure 3f, four laser beams along $\theta_{FF} = 86°$, 93°, 266°, and 273° can be clearly seen. This experimental observation and the numerical results match very well. The differences between the far-field patterns of quadrupole microdisks with and without channeling waveguide confirms again that the chiral resonances in islands have been generated by connecting a waveguide to the chaotic sea.

While the formation of optical chirality in islands has been numerically and experimentally verified, the underlying mechanism is still not very clear. In a chaotic microcavity, due to the reciprocity, the modes in the CCW domain of phase space have the same frequencies as their counterparts in the CW domain. And the tunneling from stable islands to the chaotic sea is the same as its reverse process. According to the Husimi map and the PSOS, the uncoupled stable mode in the CW and the CCW domain of phase space are widely separated. Since the tunneling probability is inversely exponentially dependent on the separation distance in phase space, the tunneling between CW and CCW stable modes can be neglected. Contrarily, based on the nature of chaotic sea, the coupling between CW and CCW chaotic modes must be taken into account. Therefore, by defining the quantities Ω_{is} and Ω_{ch} as the complex-valued dimensionless frequencies of the uncoupled stable modes and chaotic modes, the formation of chirality in stable islands can be qualitatively understood with the following 4 × 4 non-Hermitian Hamiltonian.[17–19]

$$H = \begin{vmatrix} \Omega_{is} & V & 0 & 0 \\ V & \Omega_{ch} & A & 0 \\ 0 & B & \Omega_{ch} & V \\ 0 & 0 & V & \Omega_{is} \end{vmatrix} \tag{1}$$

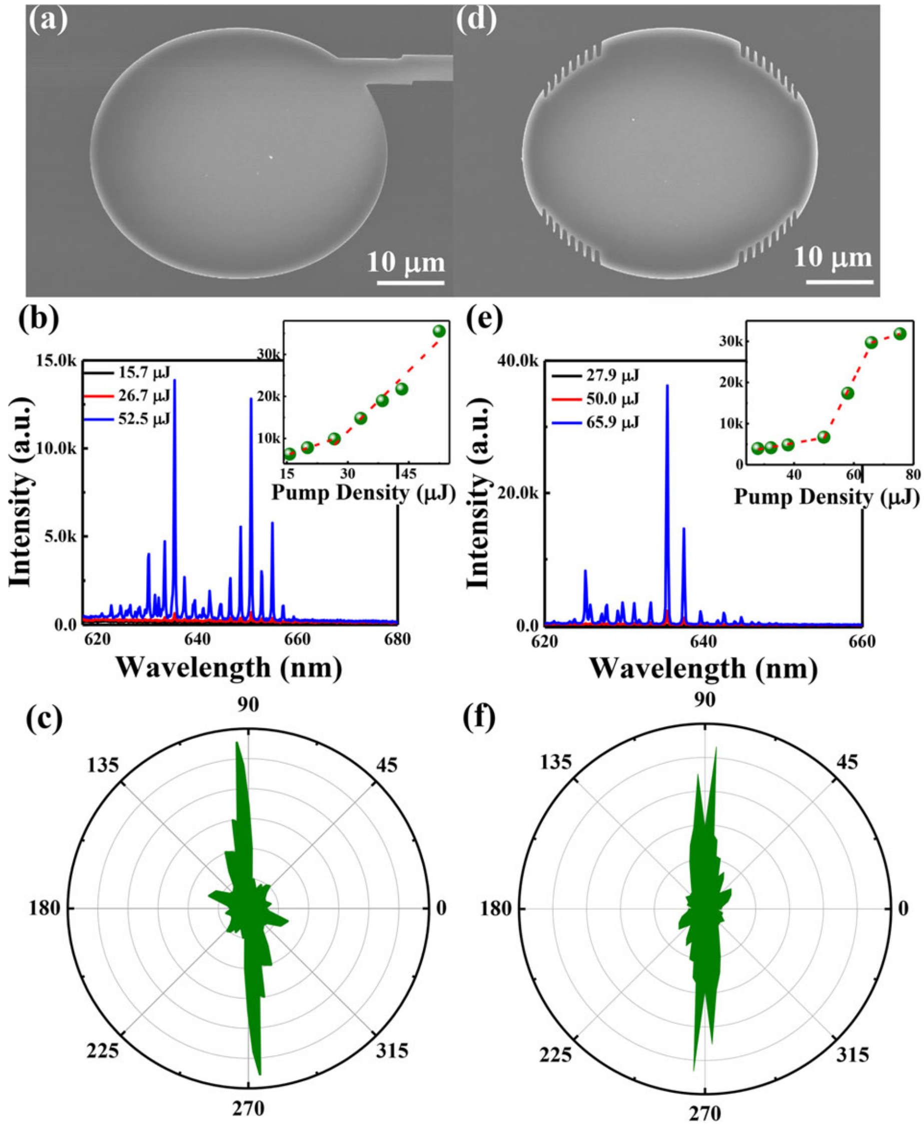

Figure 3. The experimental verification of chiral laser emission from a WCQM. a) Top-view SEM image of the WCQM. b) The emission spectrum below and above threshold. Inset shows the dependence of output intensity on the pumping power. c) FFP of diamond mode in WCQM. d) Top-view SEM image of conventional quadrupole microdisk. e) The emission spectra at different pumping powers. Inset is the L-I curve. f) The experimentally recorded FFPs. The changes of FFPs in (c) and (f) clearly show the formation of chirality after the connection of channeling waveguide.

Here, the real-valued quantity V is the coupling element describing the tunneling between the chaotic mode and the regular mode in the stable island. The chaotic-to-regular tunneling occurs with exactly the same rate than the regular-to-chaotic tunneling, because both processes are related by time-reversal symmetry. The complex-valued quantity A and B relate to the coupling from CW components to CCW components and its reversal process. Then, the eigenvalues of the above Hamiltonian are

$$\Omega_{\pm,\sigma} = \frac{\Omega_{is} + \Omega_{ch} + \sigma\sqrt{AB}}{2} \pm \sqrt{V^2 + \left(\frac{\Omega_{is} - \Omega_{ch} - \sigma\sqrt{AB}}{2}\right)^2} \quad (2)$$

with $\sigma = \pm 1$. The non-normalized eigenvectors are

$$\psi_{\pm,\sigma} = \begin{pmatrix} \sqrt{A} \\ \Delta_{\pm,\sigma}\sqrt{A} \\ \sigma\,\Delta_{\pm,\sigma}\sqrt{B} \\ \sigma\sqrt{B} \end{pmatrix} \quad (3)$$

Here, $\Delta_{\pm,\sigma}$ is the abbreviation of $\Delta_{\pm,\sigma} = \frac{\Omega_{\pm,\sigma} - \Omega_{is}}{V}$. In the spirit of the definition of the chirality,[18,19] we define the chirality of an eigenvector $\Psi = (\Psi_1, \Psi_2, \Psi_3, \Psi_4)$ as

$$\alpha_2 = 1 - \frac{min\left\{|\psi_1|^2 + |\psi_2|^2, |\psi_3|^2 + |\psi_4|^2\right\}}{max\left\{|\psi_1|^2 + |\psi_2|^2, |\psi_3|^2 + |\psi_4|^2\right\}} \quad (4)$$

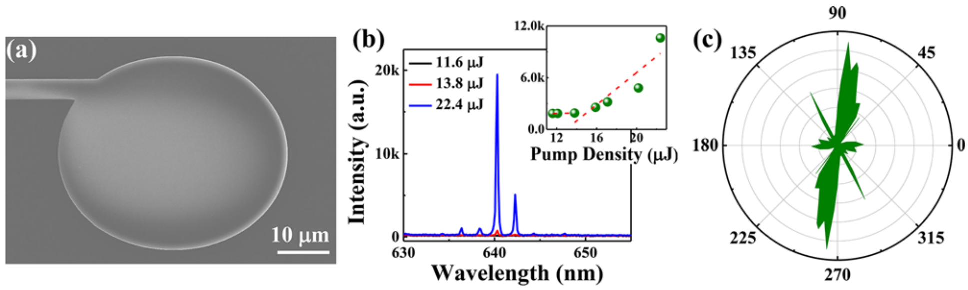

Figure 4. Chiral laser emissions from a WCQM with channeling waveguide at $\phi = 0.799\pi$. a) Top-view SEM image of the microdisk. b) The emission spectra at different pumping powers. Inset is the output intensity as a function of pumping power. c) The FFP of lasers along diamond orbit.

Plugging in the eigenvectors (3), we find

$$\alpha_2 = 1 - \frac{min\{|A|, |B|\}}{max\{|A|, |B|\}} \tag{5}$$

As the channeling waveguide breaks the mirror reflection symmetry of quadrupole cavity, the backscattering is in general asymmetric, that is, $|A| \neq |B|$ and thus the chirality within stable islands has been generated. Note that the chirality in (5) is exactly the same that we would get from the subsystem of chaotic modes alone. In that situation, the chirality is transported through the dynamical barriers.

Then the formation of chirality in stable islands has become clear. According to Equations (1) and (5), the chirality is mainly caused by the asymmetric scattering in the chaotic sea, which is conducted to the regular modes in stable islands via the tunneling from chaotic sea to stable islands. In Figure 3a, the channeling waveguide is along the direction $\phi = 0.201\ \pi$. Similar to the spiral microcavity,[34–36] the scattering from CCW direction to CW direction is stronger than its reverse process at the waveguide-microdisk joint position. Thus CW dominated chiral laser modes have been generated. Following the above physical picture, if the waveguide-microdisk joint position is switched to $\phi = 0.799\ \pi$, the scattering from CW direction to CCW direction becomes much stronger than the reversed process. Thus, the propagating directions of diamond modes in stable islands shall also be changed from CW direction to CCW direction. Based on this prediction, we thus experimentally fabricated such a microdisk and characterized its lasing properties. **Figure 4**a shows the top-view SEM image of the microdisk. Except the direction of waveguide, all the other parameters are the same as Figure 3a. By changing the pumping power, the transition from photoluminescence to discrete narrow peaks and the increase in power slope in the inset of Figure 4b confirmed the lasing actions along the diamond modes. Figure 4c shows far-field angular distributions of lasers in stable islands. Two directional laser emissions were observed at $\theta_{FF} \approx 84°$ and 264° in the far field, whereas the other two beams at $\theta_{FF} \approx 96°$ and 276° disappeared. This FFP matches the numerical results in Figure S11, Supporting Information (see part-VII, Supporting Information) very well and is exactly the same as what we have predicted from the theoretical model. Therefore, we can confirm that the asymmetric scattering in chaotic sea can be transported through the dynamical barriers and control the chirality of resonances in stable islands.

Note that the above observation is not limited in low refractive index WCQMs. It also works well in high refractive index WCMs. As shown in part-IV, Supporting Information, we have numerically calculated the chirality of diamond modes in quadrupole WCMs as a function of refractive index. The high Q chiral resonances are well preserved in a wide range of refractive index (n ≈ 1.6–4) for almost all of optical materials. Actually, the formation of chiral resonances is also a supplemental mechanism for the near unity collection efficiency at the channeling waveguide (see part-V, Supporting Information). In addition, the cavity shape is also not restricted to quadrupole shape. Similar phenomena have been observed in oval microdisks (see part-VI, Supporting Information).

4. Conclusion

In summary, while stable islands and the chaotic sea are separated by dynamical barrier, we demonstrate that the resonances in islands can be significantly affected and controlled by perturbing the chaotic sea. By connecting a channeling waveguide, the internal wave propagation and the external FFPs of quadrupole microdisks become controllable. A 4×4 non-Hermitian Hamiltonian has been developed to explain the observations and confirm the essential roles of asymmetrical backscattering and the chaotic-to-regular tunneling. This research shall be essential for fundamental studies on quantum chaos and practical applications such as optical sensing.[20,37]

Supporting Information

Supporting Information is available from the Wiley Online Library or from the author.

Acknowledgements

This work is supported by the Shenzhen Fundamental Research Projects (JCYJ20160505175637639 and JCYJ20160427183259083), Public Platform for Fabrication and Detection of Micro-& Nano-sized Aerospace Devices, Shenzhen Engineering Laboratory on Organic-Inorganic Perovskite Devices, DFG project No. WI1986/7-1, and NSF No. DMR-1506987.

Conflict of Interest

The authors declare no conflict of interest.

Keywords

chaotic resonators, dynamical tunneling, laser resonators, microcavities, quantum chaos

Received: April 8, 2018
Revised: June 25, 2018
Published online: August 26, 2018

[1] H. Cao, J. Wiersig, *Rev. Mod. Phys.* **2015**, *87*, 61.
[2] J. U. Nöckel, A. D. Stone, *Nature* **1997**, *385*, 45.
[3] C. Gmachl, F. Capasso, E. E. Narimanov, J. U. Nöckel, A. D. Stone, J. Faist, D. L. Sivco, A. Y. Cho, *Science* **1998**, *280*, 1556.
[4] Z. Duan, Y. Wang, G. Li, S. Wang, N. Yi, S. Liu, S. Xiao, Q. Song, *Laser Photon. Rev.* **2017**, *12*, 1700234.
[5] X.-F. Jiang, C.-L. Zou, L. Wang, Q. Gong, Y.-F. Xiao, *Laser Photon. Rev.* **2016**, *10*, 40.
[6] T. Harayama, S. Shinohara, *Laser Photon. Rev.* **2011**, *5*, 247.
[7] V. A. Podolskiy, E. E. Narimanov, *Opt. Lett.* **2005**, *30*, 474.
[8] J. Yang, S.-B. Lee, S. Moon, S.-Y. Lee, S. W. Kim, T. T. A. Dao, J.-H. Lee, K. An, *Phys. Rev. Lett.* **2010**, *104*, 243601.
[9] S.-B. Lee, J. Yang, S. Moon, J.-H. Lee, K. An, *Appl. Phys. Lett.* **2007**, *90*, 041106.
[10] S. Löck, A. Bäcker, R. Ketzmerick, P. Schlagheck, *Phys. Rev. Lett.* **2010**, *104*, 114101.
[11] Y.-F. Xiao, X.-F. Jiang, Q.-F. Yang, L. Wang, K. Shi, Y. Li, Q. Gong, *Laser Photon. Rev.* **2013**, *7*, L51.
[12] S. Shinohara, T. Harayama, T. Fukushima, M. Hentschel, T. Sasaki, E. E. Narimanov, *Phys. Rev. Lett.* **2010**, *104*,163902.
[13] Q. Song, L. Ge, B. Redding, H. Cao, *Phys. Rev. Lett.* **2012**, *108*, 243902.
[14] X. Jiang, L. Shao, S.-X. Zhang, X. Yi, J. Wiersig, L. Wang, Q. Gong, M. Lončar, L. Yang, Y.-F. Xiao, *Science* **2017**, *358*, 344.
[15] J. Wiersig, *Phys. Rev. Lett.* **2006**, *97*, 253901.
[16] Q. Song, H. Cao, *Phys. Rev. Lett.* **2010**, *105*, 053902.
[17] J. Wiersig, A. Eberspächer, J.-B. Shim, J.-W. Ryu, S. Shinohara, M. Hentschel, H. Schomerus, *Phys. Rev. A* **2011**, *84*, 023845.
[18] J. Wiersig, *Phys. Rev. A* **2011**, *84*, 063828.
[19] J. Wiersig, *Phys. Rev. Lett.* **2014**, *112*, 203901.
[20] N. Zhang, Z. Gu, S. Liu, Y. Wang, S. Wang, Z. Duan, W. Sun, Y.-F. Xiao, S. Xiao, Q. Song, *Optica* **2017**, *4*, 1151.
[21] B. Peng, Ş. K. Özdemir, M. Liertzer, W. Chen, J. Kramer, H. Yilmaz, J. Wiersig, S. Rotter, L. Yang, *Proc. Natl. Acad. Sci. U.S.A.* **2016**, *113*, 6845.
[22] M. Kim, K. Kwon, J. Shim, Y. Jung, K. Yu, *Opt. Lett.* **2014**, *39*, 2423.
[23] B. Peng, Ş. K. Özdemir, F. Lei, F. Monifi, M. Gianfreda, G. L. Long, S. Fan, F. Nori, C. M. Bender, L. Yang, *Nature Phys.* **2014**, *10*, 394.
[24] L. Feng, Z. J. Wong, R. M. Ma, Y. Wang, X. Zhang, *Science* **2014**, *346*, 972.
[25] H. G. L. Schwefel, N. B. Rex, H. E. Tureci, R. K. Chang, A. D. Stone, T. Ben-Messaoud, J. Zyss, *J. Opt. Soc. Am. B* **2004,** *21*, 923.
[26] M. J. Davis, E, J. Heller, *J. Chem. Phys.* **1981**, *75*, 246.
[27] H. Kwak, Y. Shin, S. Moon, S.-B. Lee, J. Yang, K. An, *Sci. Rep.* **2015**, *5*, 9010.
[28] S. Gehler, S. Löck, S. Shinohara, A. Bäcker, R. Ketzmerick, U. Kuhl, H-J. Stöckmann, *Phys. Rev. Lett.* **2015**, *115*, 104101.
[29] J. Kullig, J. Wiersig, *Phys. Rev. E* **2016**, *94*, 022202.
[30] J. Ryu, J.-W. Lee, C.-H. Yi, J.-H. Kim, I-G. Lee, H.-S. Kim, S.-B. Kim, K. R. Oh, C.-M. Kim, *Opt. Express* **2017**, *25*, 3381.
[31] Z. Gu, N. Zhang, Q. Lyu, M. Li, S. Xiao, Q. Song, *Laser Photon. Rev.* **2016**, *10*, 588.
[32] N. Zhang, Z. Gu, K. Wang, M. Li, L. Ge, S. Xiao, Q. Song, *Laser Photon. Rev.* **2017**, *11*, 1700052.
[33] M. Hentschel, H. Schomerus, R. Schubert, *Europhys. Lett.* **2003**, *62*, 636.
[34] G. D. Chern, H. E. Tureci, A. D. Stone, R. K. Chang, *Appl. Phys. Lett.* **2003**, *83*, 1710.
[35] J. Wiersig, S. W. Kim, M. Hentschel, *Phys. Rev. A* **2008**, *78*, 053809.
[36] J. Y. Lee, X. Luo, A. W. Poon, *Opt. Express* **2007**, *15*, 14650.
[37] W. Chen, Ö. Ş. Kaya, G. Zhao, J. Wiersig, L. Yang, *Nature* **2017**, *548*, 192.